

A NUMERICAL PROCEDURE FOR PREDICTING MULTIPLE SOLUTIONS OF A SPHERICAL TAYLOR–COUETTE FLOW

R.-J. YANG

Department of Engineering Science, National Cheng-Kung University, Tainan, Taiwan

SUMMARY

A new numerical procedure for predicting multiple solutions of Taylor vortices in a spherical gap is presented. The steady incompressible Navier–Stokes equations in primitive variables are solved by a finite-difference method using a matrix preconditioning technique. Routes leading to multiple flow states are designed heuristically by imposing symmetric properties. Both symmetric and asymmetric solutions can be predicted in a deterministic way. The current procedure gives very fast convergence rate to the desired flow modes. This procedure provides an alternative way of finding all possible stable steady axisymmetric flow modes.

KEY WORDS Navier–Stokes equations; Taylor–Couette flow; multiple solutions

INTRODUCTION

The set of Navier–Stokes equations is possessed of non-linear characteristics in nature. Furthermore, a flow solution depends on both initial and boundary conditions. Therefore, the Navier–Stokes equations allow multiple solutions under steady state conditions, such that, given a stationary boundary condition, a flow may have different steady state solutions depending on different initial or transient conditions. A typical example is the flow in a spherical gap.

Flow in the gap between a rotating inner and a stationary outer sphere can generate Taylor vortices. For the gap width of $\sigma = 0.18$ ($\sigma = (R_2 - R_1)/R_1$, R_1 and R_2 are the radii of inner and outer spheres), Sawatzki and Zierep¹ have observed non-unique flow modes at a supercritical Reynolds number ($Re = \Omega_1 R_1^2/\nu$, Ω_1 is the angular velocity of the inner rotating sphere and ν is the kinematic viscosity), namely, three steady axisymmetric and two unsteady non-axisymmetric modes. Steady modes contain either 0 (mode I), 1 (mode III), or 2 (mode IV) vortices per hemisphere near the equator; unsteady modes also contain either 1 or 2 vortices. Wimmer² showed in subsequent experiments that the flow modes can be produced by different accelerations of the inner sphere. Each mode requires a certain acceleration of the inner sphere to an angular velocity corresponding to the critical values of the Reynolds number. For the sake of clarity, Figures 1 and 2, taken from Bühler and Zierep,³ show schematically different steady flow modes at a supercritical Reynolds number and existence regions of the flow modes with respect to Reynolds number. Note that each flow mode has its own region of existence at steady state. For instance, at $Re = 600$, only 0-vortex flow exists; at $Re = 800$, 1- and 2-vortex flows exist; at $Re = 1500$, the three flow modes exist. As the Reynolds number is getting higher,

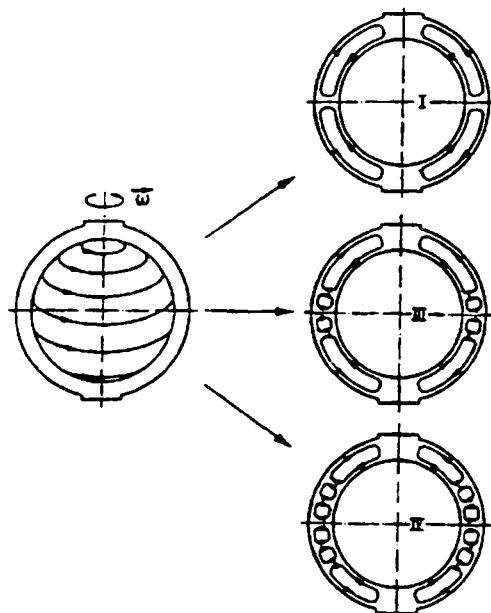


Figure 1. Different steady flow modes at a supercritical Reynolds number

the flow instability occurs and gradually transits from laminar to turbulent state. For Re greater than 11 000, only a turbulent 0-vortex flow state exists. In this study, no attempt is made to investigate the transition from laminar to turbulent problems.

Some numerical studies on the three steady axisymmetric flow modes have been made previously.⁴⁻⁸ Bartles⁴ solved the unsteady axisymmetric Navier–Stokes equations in stream-function vorticity formulation by means of a finite-difference approximation. He used a quadrant annulus ($0 \leq \theta \leq \frac{1}{2}\pi$, equator at $\theta = 0$, pole at $\frac{1}{2}\pi$) as a computation domain and imposed equatorially symmetric boundary conditions. For the gap width of $\sigma = 0.18$, he could not obtain 1-vortex flow without arbitrary disturbances of the symmetry near the equator. The other two steady modes, 0- and 2-vortex flows, were simulated through straightforward calculations. Marcus and Tuckerman⁵ used the same formulation while the equations were solved by a pseudospectral method. Their numerical computations were carried out in the whole domain ($-\frac{1}{2}\pi \leq \theta \leq \frac{1}{2}\pi$). By controlling the accelerations of the inner sphere, they were the first to reproduce 1-vortex flow as a solution of an initial-value problem directly from the basic flow. As with the long development time for experiments, a long

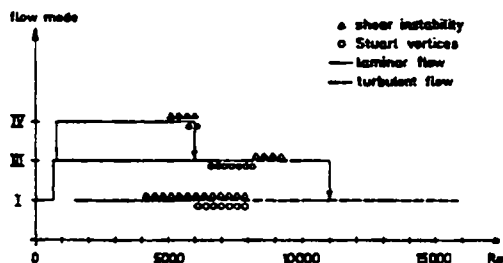


Figure 2. Existence regions of the flow modes

computation time was also needed for this mode. Shrauf⁶ used the continuation method to investigate how the instability of the spherical Couette flow depends on the gap size. Bühler⁷ presented a comprehensive investigation of a spherical gap flow, $\sigma = 0.154$, with an initial value code based on an explicit finite difference method. He discovered for the first time that, within the non-existence range of the symmetric 1-vortex mode, a similar 1-vortex stable mode asymmetric with respect to the equatorial plane can exist. The asymmetric mode consists of two Taylor vortices, only slightly larger than the other and straddling the equator. This is interesting, since the boundary conditions are always symmetric with respect to the equator. The existence of such asymmetric modes is confirmed by his experiments. Mamun and Tuckerman⁸ devised a unified computational approach to study the bifurcation-theoretic origin of Bühler's asymmetric states. They found that the asymmetric branch originates from pitchfork bifurcation; its stabilization occurs via a subsequent subcritical Hopf bifurcation.

The state attained by the flow depends on its history, especially on the transient acceleration of the inner sphere from rest to its final rotation state, and on the kind of disturbances permitted by experimental set-up or numerical schemes. By closely mimicking laboratory experiments, the steady flow modes can be simulated numerically by solving the full-time dependent Navier–Stokes equations. Although the free flow modes are axisymmetric and symmetric with respect to the equator at steady states, the whole domain ($-\frac{1}{2}\pi \leq \theta \leq \frac{1}{2}\pi$) is required in the case of simulating 1-vortex flow since the transition process of the flow was found to be breaking symmetry at the equator.⁵ The advantage of solving the full-time dependent Navier–Stokes equations (initial- and boundary-value equations) is that one can examine the physics associated with the transition process. The disadvantage is that it requires many time-steps if the particular physics associated with the transition is slow. Mamun and Tuckerman⁸ proposed a steady-state solver coupled with a continuation method that they can find all the steady states and locate bifurcation points. They used the Newton's method together with a matrix preconditioning to make the continuation method inexpensive. Both the southern and the northern hemispherical shells are required in the domain of the calculation.

In this study, a technique is proposed to simulate the three steady axisymmetric laminar and the asymmetric flow modes. In the numerical simulation, only half the domain ($0 \leq \theta \leq \frac{1}{2}\pi$) is required for simulating the axisymmetric flow modes, hence saves half the computational cost. Matrix preconditioning technique is applied to the Navier–Stokes equations for a faster convergence rate to the steady state. The effect of the preconditioning parameters on the convergence rate is investigated. A method, by means of fictitious symmetric boundary conditions, defining routes to each flow mode is introduced without taking into account the transition process. The asymmetric flow mode can be similarly simulated, however, both the northern and southern spherical shells are included in the computational domain. The computational procedure also provides a fast way of finding all possible steady axisymmetric flow modes. The present solutions, in terms of friction torques and vortex sizes, show excellent agreement with the experiments.

GOVERNING EQUATIONS AND NUMERICAL METHOD

The three-dimensional, incompressible Navier–Stokes equations are modified to the following set of governing equations:

$$\frac{1}{\beta} \frac{\partial p}{\partial t} + \frac{\partial u_i}{\partial x_i} = 0, \quad (1)$$

$$\frac{(\alpha + 1)u_i}{\beta} \frac{\partial p}{\partial t} + \frac{\partial u_i}{\partial t} + \frac{\partial u_i u_j}{\partial x_j} = -\frac{\partial p}{\partial x_i} + \frac{\partial \tau_{ij}}{\partial x_j}, \quad (2)$$

where t is time; x_i are the Cartesian co-ordinates; u_i are corresponding velocity components; p is the pressure; and τ_{ij} are the stress tensors. The parameters α and β , according to Turkel,⁹ are introduced to precondition the Navier–Stokes equations and allow for a faster convergence to the steady state. This formulation is an extension of Chorin's artificial-compressibility method.¹⁰ The artificial-compressibility method added an artificial time derivative of the pressure to the continuity equation together with a parameter β (i.e. let $\alpha = -1$ in (2)). The method has been applied successfully to investigate complex internal flow problems.^{11–13}

The equations are then transformed to a general co-ordinate system in which the general co-ordinates ξ_i are related to the Cartesian co-ordinate x_i by

$$\xi_i = \xi_i(x, y, z). \quad (3)$$

In the generalized curvilinear co-ordinates, the governing equations in conservation-law form are expressed as

$$M \frac{\partial}{\partial t} \hat{D} + \frac{\partial}{\partial \xi_i} (\hat{E}_i - \hat{\Gamma}_i) = 0. \quad (4)$$

Preconditioning matrix M , pressure and velocity vector \hat{D} , flux vector \hat{E} , and viscous diffusion vector $\hat{\Gamma}$ are described by

$$M = \begin{bmatrix} \beta^{-1} & 0 & 0 & 0 \\ (\alpha + 1)u\beta^{-1} & 1 & 0 & 0 \\ (\alpha + 1)v\beta^{-1} & 0 & 1 & 0 \\ (\alpha + 1)w\beta^{-1} & 0 & 0 & 1 \end{bmatrix}, \quad \hat{D} = \frac{D}{J} = \frac{1}{J} \begin{bmatrix} p \\ u \\ v \\ w \end{bmatrix}, \quad \hat{E}_i = \frac{1}{J} \begin{bmatrix} U_i \\ uU_i + L_{i1}p \\ vU_i + L_{i2}p \\ wU_i + L_{i3}p \end{bmatrix},$$

$$\hat{\Gamma}_i = \frac{v}{J} (\nabla \xi_i \cdot \nabla \xi_j) \frac{\partial}{\partial \xi_j} (0, u, v, w)^T$$

where J is the Jacobean of co-ordinate transformation, and

$$U_i = L_{i1}u + L_{i2}v + L_{i3}w,$$

$$L_{i1} = (\xi_i)_x, \quad L_{i2} = (\xi_i)_y, \quad L_{i3} = (\xi_i)_z$$

are the contravariant velocities and the metrics of transformation respectively.

The governing equations are replaced by an implicit time difference approximation (backward-difference). Non-linear numerical fluxes at the implicit time level are linearized by Taylor expansion; then, spatial difference approximations (central-difference) are introduced. The result is a system of multidimensional, linear, coupled difference equations for the dependent variables at the implicit time level. To solve these equations, the approximate-factorization or ADI scheme^{14,15} is used. This technique leads to the following system of coupled linear difference equations

$$\begin{aligned} (M + \Delta t L_\xi) \Delta D^* &= RHS, \\ (M + \Delta t L_\eta) \Delta D^{**} &= M \Delta D^*, \\ (M + \Delta t L_\zeta) \Delta D &= M \Delta D^{**}, \end{aligned} \quad (5)$$

where

$$\begin{aligned} L_{\xi_i} &= J \delta_{\xi_i} (\hat{A}_i - \hat{\Gamma}_i), & RHS &= -\Delta J \sum \delta_{\xi_i} (\hat{E}_i - \hat{\Gamma}_i), \\ \hat{A}_i &= \partial \hat{E}_i / \partial D, & \Delta D &= D^{n+1} - D^n, \end{aligned}$$

ΔD^* and ΔD^{**} are intermediate solutions. The system of equation (5) can be written in narrow block-banded matrix structures and be solved by a standard LU decomposition method.

INITIAL AND BOUNDARY CONDITIONS

At a supercritical Reynolds number, the final steady states of the spherical Taylor-Couette flow depend on the accelerating history of the inner sphere and initial conditions. The present numerical algorithm uses a preconditioning method and thus transient history is different from the realistic situation. Disregarding the transient accuracy, the current work is to find route leading to steady 0-, 1- and 2-vortex flows with a faster convergent rate to the steady states. The computation is conducted in a quadrant annulus $0 \leq \theta \leq \frac{1}{2}\pi$. The initial conditions for all calculations (except some special cases) are given as follows: linear velocity profile across the gap in the circumferential direction, zero velocity components in the meridional plane, and zero static pressure in the entire domain.

The modified Navier-Stokes equations have a symmetric hyperbolic system. The preconditioning matrix is positive definite ($\beta > 0$). The appropriate number of boundary conditions is the same as that for the original Navier-Stokes equations. To make the problem well-posed, the following boundary conditions are used: reflection-symmetric condition is applied at equator and pole, no-slip condition is used on inner and outer sphere surfaces, normal pressure gradient on both sphere surfaces is balanced by centrifugal and viscous forces, and a reference pressure is set at a specified point in the computation domain.

COMPUTATIONAL PROCEDURE AND RESULTS

Spherical Taylor-Couette flow is characterized by two parameters: the Reynolds number, (Re), and the gap width, (σ). The current computations are performed for $\sigma = 0.18$ and $Re \leq 1500$. Numerical convergence is checked by monitoring the friction torques acting on inner and outer sphere surfaces. At a steady state, the friction torques are equal in magnitude and the numerical residual has to drop three orders of magnitude. To make sure the steady-state solutions are independent of mesh distributions, two grid systems were tested for the case of $Re = 1500$: 111×51 and 81×41 ($J \times K$, J and K are number of mesh points in azimuthal and radial direction respectively). Both computed solutions were nearly identical to each other. Therefore, 81×41 grid system is used throughout these calculations. Dense mesh is used in the regions where the flow gradient is expected to be large. For example, in the near wall regions and the regions where the Taylor vortices are formed.

Preconditioning parameters (α and β) remained to be specified. The proper choice of the parameters can enhance convergent rate to steady states. A parametric study is therefore investigated to demonstrate this effect. Figures 3 and 4 show the residual histories with different values of α and β for $Re = 600$. In Figure 3, $\alpha = 1$, different values of β result in different convergent rate. For $\beta = 1$ gives the best convergent rate, in contrast to $\beta = 3$ which gradually deteriorates the solution. In Figure 4, $\beta = 1$, different values of α also yields different convergent rate. It is shown in Reference 9, for an inviscid equation, $\alpha = 1$ makes the acoustic sound speed isotropic and independent of the flow velocity. The current investigation of convergence for viscous flow calculations also has the same trend as for the inviscid equation. On the basis of this investigation, all calculations performed in this study use $\alpha = \beta = 1$.

In the region near the pole, local flow is similar to that which occurs in the gap between a rotating disc and a stationary housing. In the region near the equator, local flow is similar to that of cylindrical Taylor-Couette flow. Because of the Eckman pumping effects, centrifugal forces drive fluid along the inner rotating sphere from the pole toward the equator. Near or at the equator plane (depending on flow mode), the fluid is deflected outwards and moved back to the pole in the vicinity of the outer sphere. It

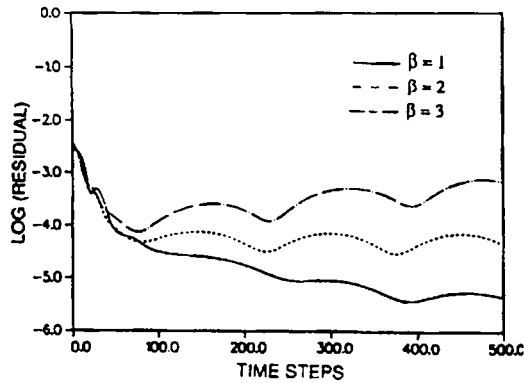


Figure 3. Residual history for $Re = 600$ with $\alpha = 1$

should be noted that each flow mode has its own region of existence at steady state. The following discussions are based on the assumption that each flow mode exists at a given Reynolds number in each category. Routes leading to these flow modes are described below.

Route to 0-vortex flow

Using initial and boundary conditions depicted in an earlier Section, the current numerical method converges to a 0-vortex flow. It has to be noted that the friction torque for both inner and outer spheres has to reach a constant at steady state. Figure 5 shows the results for $Re = 600$. It clearly shows that after $NT = 300$, the flow reaches an equilibrium state (i.e. both inner and outer friction torques are equal). If the flow mode does not exist at a given Reynolds number, an equilibrium state may be obtained during the process of the calculation; however, the friction torque is not a constant during the time interval. Eventually, the friction torque reaches a constant and then another steady flow mode is formed. An example will be given later.

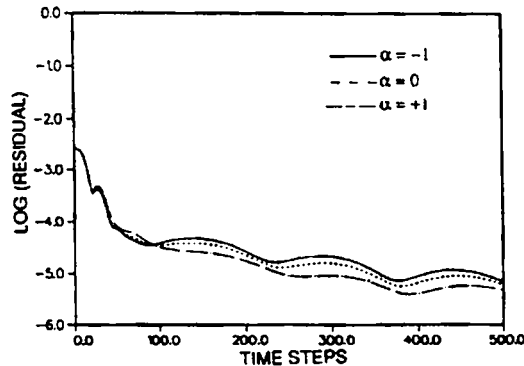


Figure 4. Residual history for $Re = 600$ with $\beta = 1$

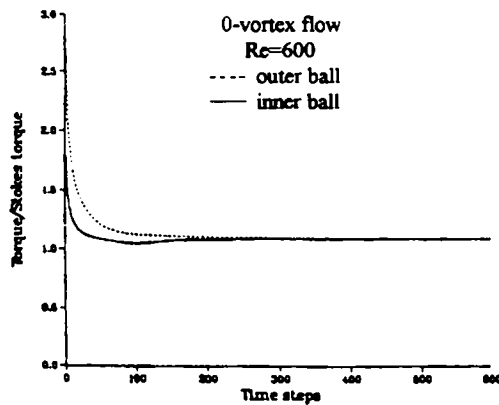


Figure 5. Frictional torque history for $Re = 600$

Route to 1-vortex flow

Experimental observations indicated that vortex size near the equator of 1-vortex flow has the same order of the gap width's magnitude. The vortex near the equator is separated from the major portion of the meridional flow through a dividing streamline. Local flow on either side of the streamline reveals symmetric character. For the numerical simulation of the 1-vortex flow, a radial line at one gap width distance away from the equator is chosen as a fictitious inner symmetric boundary; there flow variables are treated as symmetric. Using conditions described in an earlier section and the inner symmetric treatment, a 'rough' 1-vortex flow can be simulated. With the 'rough solution' as the initial condition and taking out the treatment at the specified radial line, the current numerical method converges to a 1-vortex flow. In the calculation of Reference 4, although the half domain ($0 \leq \theta \leq \frac{1}{2}\pi$) was used, one has to disturb the flow near the equator constantly to form the 1-vortex flow. In contrast, the current approach has a clear location to impose the fictitious symmetry condition. In the calculations of Reference 5, the whole domain ($-\frac{1}{2}\pi \leq \theta \leq \frac{1}{2}\pi$) is required since the transition process of the 1-vortex flow revealed symmetry breaking at the equator. Furthermore, one has to control the rotating history for a long time to form the 1-vortex flow during the transient accurate calculation. With the current approach, only half domain is required and there is no need to control the rotating history of the inner sphere. The treatment at the chosen fictitious boundary during the initial calculation creates a necessary state for 1-vortex flow to exist.

Routes to 2-vortex flow

There are two routes that can lead to a steady 2-vortex flow. First a similar treatment as with 1-vortex flow is applied to the 2-vortex flow simulation. In this case two radial lines are chosen as fictitious inner symmetric boundaries. The separation distance along the two radial lines and the equator is about one gap width each. Computation with conditions given in an earlier section and the inner symmetric treatment at the two radial lines can lead to a 'rough' 2-vortex flow. Taking out the treatment at the two specified radial lines and using the rough solution as the initial condition, the current numerical method converges to a steady 2-vortex flow. This treatment toward the final steady 2-vortex flow is called forced transition. Another route is called free transition. In this case, a straightforward calculation using initial and boundary conditions given earlier can converge to a steady 2-vortex flow. In the process of the free transition, it is observed that the friction torque for both inner and outer spheres is in an equilibrium state but is not a constant with respect to time during a time interval. Figure 6 shows an

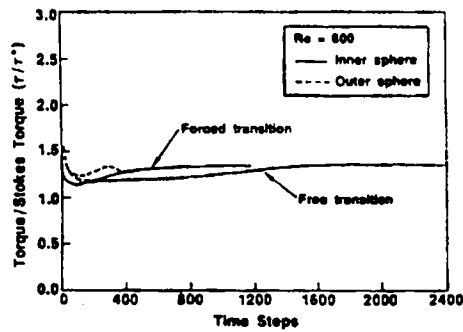


Figure 6. Convergent history toward 2-vortex flow

example of convergent histories for both forced and free transition for the case of $Re = 800$. In the case of free transition, the flow reaches an equilibrium state after 300 time steps ($NT = 300$). However, the friction torque varies with respect to time until $NT = 1600$. In the case of forced transition, the first 300 time steps were treated as having inner symmetric boundaries and continuing the calculation, the flow converges to a steady 2-vortex flow after $NT = 500$. It is obvious that the case of the forced transition led to a much faster convergent rate toward a steady state. One has to be cautious in judging whether a solution is converged. To clarify this question, Figure 7 shows the residual history as well as the friction torque for both the inner and outer spheres. The calculation was performed with a straightforward computation for $Re = 800$. It is observed that an equilibrium state is reached after $NT = 300$. However, the residuals gradually increase from $NT = 500$ to $NT = 1200$. Therefore, a constant frictional torque and a drop of three order of magnitude in the residual are required for a convergent solution.

The three steady flow modes behave quite differently near the equator. Figure 8(a) gives velocity vectors on meridional plane and Figure 8(b) gives circumferential velocity component at the equator for the case of $Re = 1500$. Taylor vortices for 1- and 2-vortex flows are clearly shown. The circumferential velocity profiles at the equator are quite different due to the Taylor vortices. Figures 9 and 10 give circumferential skin friction and azimuthal pressure gradient coefficients. Wild differences are clearly shown within $\theta \leq 40^\circ$. From Figure 8(a) and Figure 10, it is interesting to note that the turning directions of the Taylor vortices are consistent with the pressure gradient in the theta direction along the inner sphere surface. In Figures 11 and 12, the current results (friction torques and vortex

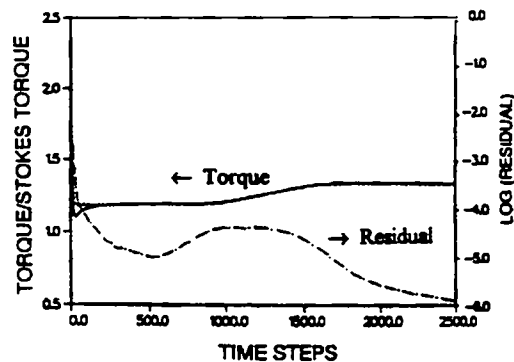


Figure 7. Frictional torque and residual history for 2-vortex flow

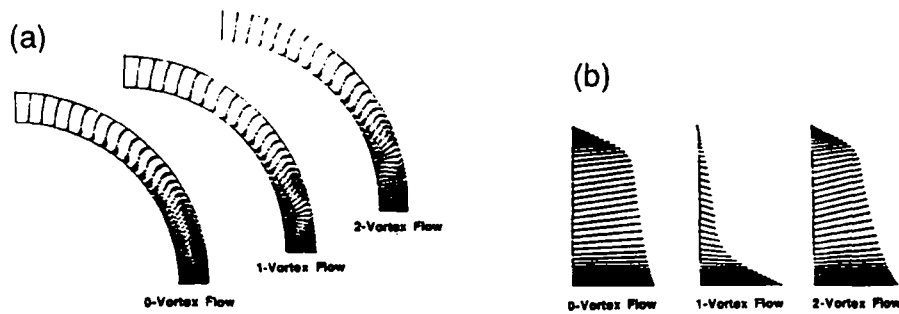


Figure 8. (a) Velocity vectors on meridional plane ($Re = 1500$). (b) Circumferential velocity profiles at equator ($Re = 1500$)

sizes) agree quite well with the Marcus⁵ calculations and Wimmer² measurements. From Figure 11, region of existence for the three flow modes is clearly shown. The 0- and 2-vortex flows lie on the same solution branch, and the 1-vortex flow lies on a separate branch.

GENERALIZATION OF THE USE OF FICTITIOUS BOUNDARY CONDITIONS

The computational procedure described previously can be generalized to other flow geometries without prior knowledge of the final answer. Before giving an example, the following comments are made.

1. The vortex size in a spherical gap is almost in square form. Thus we can place fictitious boundaries along the θ - direction at $n \times \sigma$, where n is the number of fictitious boundaries. In doing so, we can generate n vortices in a spherical shell deterministically.
2. For the gap width $\sigma = 0.18$, $Re = 1000$, we perform numerical experiments by setting value of n from 1 to 4. As described in the previous section, by imposing $n = 1$ and $n = 2$ during the initial 'seeding' process, then take out the imposed fictitious boundary treatments, at the steady state we obtain 1- and 2-vortex flow solutions respectively. By imposing $n = 3$ and $n = 4$, we can seed the 3- and 4-vortex flows as initial conditions. Taking out the imposed boundaries and continue the computation, then we obtain a 2-vortex flow solution at the steady state. It is seen that no matter how many vortices being created for the initial condition, a steady 2-vortex flow solution will be obtained.

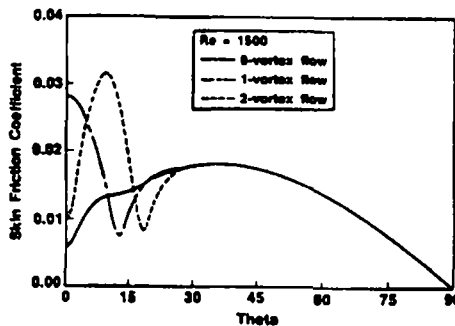


Figure 9. Circumferential skin friction coefficient on inner sphere surface

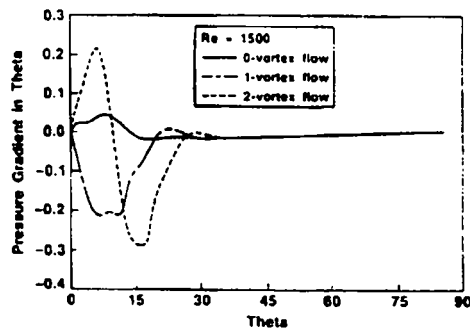


Figure 10. Azimuthal pressure gradient coefficient on inner sphere surface

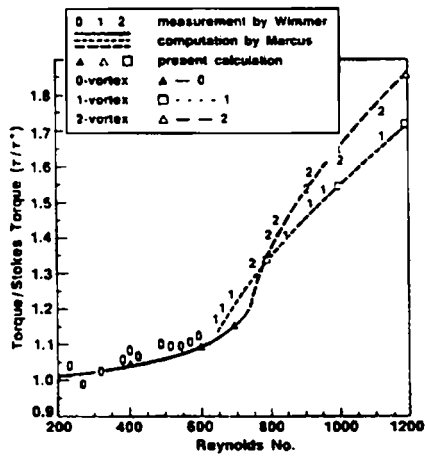


Figure 11. Frictional torques

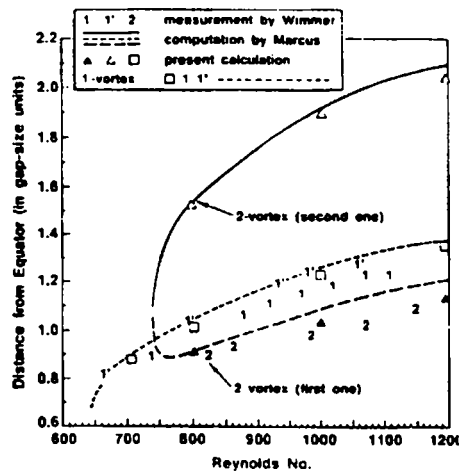


Figure 12. Vortex sizes

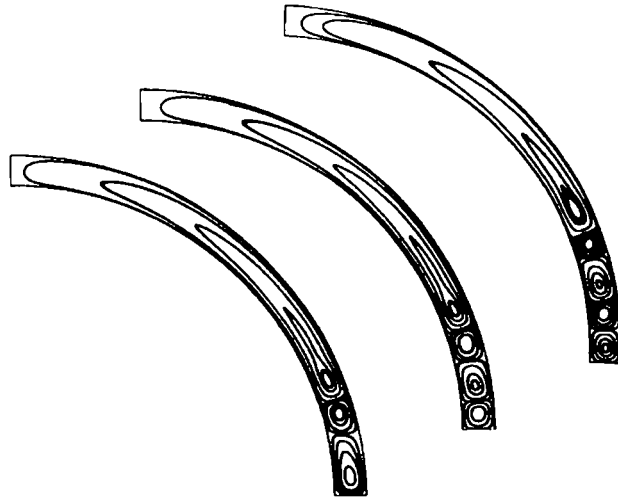


Figure 13. Streamline patterns for all possible axisymmetric flow modes, $\sigma = 0.1$, $Re = 2500$

3. In principle, we can arbitrarily apply any number of fictitious boundaries during the initial seeding process. However, Taylor vortices are observed, from experiments, to occur near the equator within 30° along the θ -direction. Therefore, there is no need to seed the vortices beyond the 30° location.

Based upon the above comments, we perform a calculation in which no prior answer is known. The flow geometry and the Reynolds number are $\sigma = 0.1$ and $Re = 2500$ respectively. By imposing $n = 1, 2, 3$ and 4 , we obtain steady solutions for 3-vortex, 2-vortex, 3-vortex and 4-vortex flow respectively. For $n > 4$, we can only obtain a steady 4-vortex flow solution. Under the present computation procedure, three steady axisymmetric flow modes are found, namely, 2-, 3- and 4-vortex flows. The streamlines of these solutions are shown in Figure 13. The computed ratio of the frictional torque to the Stokes torque is 1.53, 1.65 and 1.71 respectively. This computation procedure provides an alternative way of finding all possible steady flow modes.



Figure 14. Streamline of the asymmetric 1-vortex flow mode, $\sigma = 0.154$, $Re = 1500$

It would be interesting to extend the current technique to simulate the asymmetric 1-vortex flow discovered by Bühler.⁸ The flow conditions are: the gap width $\sigma = 0.154$, and $Re = 1500$. Since the flow is asymmetric with respect to the equator, both the southern and northern spherical shells are included in the computation domain. Bühler has a 'recipe' to obtain the asymmetric solution. First, a sudden acceleration from rest to $Re = 1850$ will produce a supercritical 0-vortex state. Then by decreasing Re , the asymmetric 1-vortex state is obtained. His procedure will show the physical vortex transition between different flow states. If applying the present seeding procedure, then a treatment in the fictitious boundary is imposed in the southern hemisphere at the distance about 2σ away from the equator. This asymmetric seeding will produce a rough initial asymmetric 1-vortex flow. Taking out the imposed fictitious boundary treatment and preceding the computation, a steady asymmetric 1-vortex flow solution can be obtained. Figure 14 shows the streamline of the final steady solution.

CONCLUSION

A new technique to simulate Taylor vortices in a spherical gap has been developed and tested. The incompressible Navier–Stokes equations are solved by using a matrix preconditioning technique. The non-unique steady flow modes associated with the Taylor vortices are simulated in special ways. Routes leading to different vortex flows are designed heuristically. Fictitious symmetric boundaries near the equator are imposed during a time of the calculation and the choice of location of the fictitious boundaries is determined by the desired flow mode being simulated. The imposition of the fictitious symmetric boundaries during the initial calculation generates the state suitable for the desired flow mode to exist. After taking out the fictitious boundaries, the flow settles down into its own attractor. By this method, all possible stable steady axisymmetric flow modes can be simulated by using half domain, i.e. $0 \leq \theta \leq \frac{1}{2}\pi$. Therefore, computational cost is saved 50 per cent compared with that using the whole domain. The procedure also provides a fast way of finding all possible stable steady axisymmetric flow modes. An asymmetric solution can also be predicted by a deterministic way. The current numerical technique converges to desired flow modes very fast.

It is worthwhile noting limitations of the present computation method. They are listed in the following. (1) Similar to continuation methods, the present method computes steady-state flow modes only. Here, a matrix preconditioning technique is used. Therefore, no physical meaning can be ascribed to the evolution of the flow from the initial state to the final state. (2) The final states may or may not be linearly unstable, and the present method can not determine the stability since pseudotime is used in the integration. (3) Unlike continuation methods, which produce bifurcation diagrams, the present method may require extensive parametric study to obtain a global picture of a flow. (4) After computing one or more converged, steady states at a fixed value of the control parameter with this method (by starting with different initial and boundary conditions), it seems difficult to know whether all of the steady states at that fixed control parameter have been found. This is true for the continuation method as well. However, if one is systematic, at least it is known that one has found all solutions that bifurcate from the main, secondary, tertiary, etc., branches at bifurcation parameter numbers less than some upper bound. (5) Some unstable steady spherical Taylor–Couette flows may exist. Calculating unstable steady states by the present time integration is, of course, impossible. The present method only provides a rapid way of calculating stable steady states. With continuation methods, if one can find the branch or its bifurcation point, then one can compute the solution.

ACKNOWLEDGMENT

Special thanks is due to Professor P. S. Marcus of the University of California, Berkeley, U.S.A. for his valuable comments on the manuscript. This work is partially supported by the National Science Council, Taiwan, under grant number NSC-84-2212-E006-024.

REFERENCES

1. O. Sawatzki and J. Zierep, *Acta Mechanica*, **9**, 13–35 (1970).
2. M. Wimmer, 'Experiments on a viscous fluid flow between concentric rotating spheres', *J. Fluid Mech.*, **79**, 317–335 (1976).
3. K. Bühler and J. Zierep, 'Transition to turbulence in a spherical gap', in *Proc. 4th Int. Sym. on Turbulent Shear Flows*, 16.1–16.6, 1983.
4. F. Bartels, 'Taylor vortices between two concentric rotating spheres', *J. Fluid Mech.*, **119**, 1–25 (1982).
5. P. S. Marcus and L. S. Tuckerman, 'Simulation of flow between concentric rotating spheres, Part 1—steady states and Part 2—transitions', *J. Fluid Mech.*, **185**, 1–65 (1987).
6. G. Schrauf, 'The first instability in spherical Taylor–Couette flow', *J. Fluid Mech.*, **166**, 287–303 (1986).
7. K. Bühler, 'Symmetric and asymmetric Taylor vortex flow in spherical gaps', *Acta Mechanica*, **81**, 3–38 (1990).
8. C. K. Mamun and L. S. Tuckerman, 'Asymmetry and Hopf bifurcation in spherical Couette flow', *Phys. Fluids*, **7**(1), 80–91 (1995).
9. E. Turkel, 'Preconditioned methods for solving the incompressible and low speed compressible equations', *J. Comput. Phys.*, **72**, 277–297 (1987).
10. A. J. Chorin, 'A numerical method for solving incompressible viscous flow problems', *J. Comput. Phys.*, **2**(12), 12–26 (1967).
11. D. Kwak, J. Chang, S. P. Shanks, and S. Chakaravarthy, 'A three-dimensional incompressible Navier–Stokes flow solver using primitive variables', *AIAA J.*, **24**(3), 380–396 (1986).
12. J. L. C. Chang, D. Kwak, S. E. Rogers, and R.-J. Yang, 'Numerical simulations of incompressible flows and an application to the space shuttle main engine', *Int. J. Numer. Methods Fluids*, **8**, 1241–1268 (1988).
13. R.-J. Yang, J. L. C. Chang, and D. Kwak, 'Navier–Stokes flow simulation of the space shuttle main engine hot gas manifold', *AIAA J. Spacecraft Rocket*, **29**(2), 253–259 (1992).
14. R. M. Beam and R. F. Warming, 'An implicit finite-difference algorithm for hyperbolic systems in conservation-law form', *J. Comput. Phys.*, **22**, 87–110 (1976).
15. W. R. Briley and H. McDonald, 'Solution of the multidimensional compressible Navier–Stokes equations by a generalized implicit method', *J. Comput. Phys.*, **24**, 372–397 (1977).